LETTER • OPEN ACCESS

Decoupling between ecosystem photosynthesis and transpiration: a last resort against overheating

To cite this article: Christopher Krich *et al* 2022 *Environ. Res. Lett.* **17** 044013

View the article online for updates and enhancements.

You may also like

ENVIRONMENTAL RESEARCH
LETTERS

LETTER

Decoupling between ecosystem photosynthesis and transpiration: a last resort against overheating

Christopher Krich[2] ⓘ, Miguel D Mahecha[1,3] ⓘ, Mirco Migliavacca[1,8], Martin G De Kauwe[4] ⓘ, Anne Griebel[5], Jakob Runge[6,7] ⓘ and Diego G Miralles[2,*] ⓘ

[1] Max Planck Institute for Biogeochemistry, 07745 Jena, Germany
[2] Hydro-Climate Extremes Lab (H-CEL), Ghent University, Ghent 9000, Belgium
[3] Remote Sensing Centre for Earth System Research, Leipzig University, 04103 Leipzig, Germany
[4] School of Biological Sciences, University of Bristol, Bristol, United Kingdom
[5] Hawkesbury Institute for the Environment, Western Sydney University, Locked Bag 1797, Penrith, NSW 2751, Australia
[6] German Aerospace Center, Institute of Data Science, 07745 Jena, Germany
[7] Technische Universität Berlin, Berlin 10623, Germany
[8] European Commission, Joint Research Centre, Ispra (VA) 21027, Italy
[*] Author to whom any correspondence should be addressed.

E-mail: diego.miralles@ugent.be

Abstract

Ecosystems are projected to face extreme high temperatures more frequently in the near future. Various biotic coping strategies exist to prevent heat stress. Controlled experiments have recently provided evidence for continued transpiration in woody plants during high air temperatures, even when photosynthesis is inhibited. Such a decoupling of photosynthesis and transpiration would represent an effective strategy ('known as leaf or canopy cooling') to prevent lethal leaf temperatures. At the ecosystem scale, continued transpiration might dampen the development and propagation of heat extremes despite further desiccating soils. However, at the ecosystem scale, evidence for the occurrence of this decoupling is still limited. Here, we aim to investigate this mechanism using eddy-covariance data of thirteen woody ecosystems located in Australia and a causal graph discovery algorithm. Working at half-hourly time resolution, we find evidence for a decoupling of photosynthesis and transpiration in four ecosystems which can be classified as Mediterranean woodlands. The decoupling occurred at air temperatures above 35 °C. At the nine other investigated woody sites, we found that vegetation CO_2 exchange remained coupled to transpiration at the observed high air temperatures. Ecosystem characteristics suggest that the canopy energy balance plays a crucial role in determining the occurrence of a decoupling. Our results highlight the value of causal-inference approaches for the analysis of complex physiological processes. With regard to projected increasing temperatures and especially extreme events in future climates, further vegetation types might be pushed to threatening canopy temperatures. Our findings suggest that the coupling of leaf-level photosynthesis and stomatal conductance, common in land surface schemes, may need be re-examined when applied to high-temperature events.

1. Introduction

Transpiration and photosynthesis tend to be synchronised, since they share common environmental constraints and drivers, and stomatal regulation modulates both processes (Ball *et al* 1987, Leuning 1995). For example, during conditions of high atmospheric aridity, i.e. high vapour pressure deficit (VPD), stomata close to curb water losses. On the other hand, if biochemical limitations lead to a reduction of photosynthesis, the internal leaf CO_2 concentration increases, as well causing stomata closure. During conditions of extremely high air temperatures and VPD, species have been found that continue to transpire even after photosynthetic activity is reduced to near zero, and as long as soil moisture is still sufficiently available (Schulze *et al* 1973, Ameye *et al* 2012). This behaviour, which can be described as a decoupling between photosynthesis and transpiration under heat stress, can be

hypothesised to be a plant strategy to reduce the adverse effects of too high temperatures on the plant, cooling the canopy air space via evaporation (Drake *et al* 2018). However, hydraulic traits exhibit substantial differences among species (Peters *et al* 2021). The 'transpirational cooling' strategy can thus vary strongly from species to species, and it relies on the access to water (O'sullivan *et al* 2017).

To date, evidence of such decoupling between photosynthesis and transpiration stems from experiments on individual trees, either investigating stomatal conductance at leaf scale (Schulze *et al* 1973, Ameye *et al* 2012, von Caemmerer and Evans 2015, Urban *et al* 2017) or gas exchanges on whole trees (Drake *et al* 2018). These studies showed a decrease in photosynthesis but continuous high transpiration with extreme temperatures. While most of these studies reported a vanishing decoupling as soil desiccated causing the decline in transpiration, in Drake *et al* (2018) it persisted despite omitting irrigation for a month to simulate water-limited conditions. In particular, Drake *et al* (2018) conducted measurements using whole tree chambers on 6 m tall *Eucalyptus parramattensis* trees grown in field settings. Heatwaves were simulated for four consecutive days with air temperatures exceeding 43 °C. Such studies show that soil moisture appears a determining factor. Yet, some trees might be capable to tap into sufficient soil water reserves to maintain transpiration at high temperatures even during times in which the top soil is dry. In such cases, at the ecosystem scale, a decoupling between photosynthesis and transpiration could also lead to a negative land-atmosphere feedback, cooling the boundary layer. So far, only one study has investigated this decoupling of photosynthesis and transpiration during hot spells in woody ecosystems. De Kauwe *et al* (2019) compared the mean daytime latent heat flux (LE) and daily cumulative gross primary productivity (GPP) of ecosystems experiencing maximum air temperatures exceeding 37 °C. The focus was on Australian ecosystems due to the severity of the heat events striking them and lack of evidence in FLUXNET2015 sites. A faster decline in GPP than for LE was observed at three eddy-covariance sites: Gingin (Woody Savannah, WSA), Great Western Woodlands (WSA) and Calperum (WSA). While this supported the hypothesis of a decoupling, when accounting for the influence of VPD, only Great Western Woodlands showed some (weak) sign.

An inherent difficulty when studying ecosystem-scale decoupling based on eddy-covariance data relates to the difficulties to separate the contribution of transpiration to the measured LE, and photosynthesis to the measured net ecosystem exchange. Partitioning methods for both fluxes exist (Reichstein *et al* 2012, Nelson *et al* 2020), yet it remains uncertain whether they can capture the peculiarities of ecosystem behaviour at extreme temperatures (De Kauwe

et al 2019). A more fundamental question to ask, however, is whether a decoupling shall be investigated using a correlative approach looking primarily at variable values (e.g. is GPP decreasing while LE remains high). Investigations using such approach revealed carbon and water fluxes to change by different factors comparing heat wave and non heat wave conditions (van Gorsel *et al* 2016, Griebel *et al* 2020a, 2020b). Such differences in the change of fluxes might be interpreted as a decoupling. However, as there are many co-varying influences, a correlative approach investigating the relation between photosynthesis and transpiration cannot reveal whether observed differences stem from changes in radiation, air temperature, VPD or in fact stomatal conductance. An alternative approach would be a causal analysis that reveals changes in the dependence structure among variables which is independent of variable values and takes into account co-varying variables. Such causal analysis builds upon the perspective that a change in variable *X* leads to a change in variable *Y* if a causally explainable dependence exists among *X* and *Y*. This dependence can be direct (causal) or due to a common driver or intermediate variable (spurious). If common drivers and intermediate variables are included in the analysis, causal dependencies can be distinguished from spurious ones. This type of approach alleviates the main pitfall of correlational analyses, which is their inability to distinguish between spurious and causal dependencies. Further it cannot reveal the directionality and strength of the coupling among multiple variables, particularly complex systems such as the land–atmosphere interface (Krich *et al* 2019).

A formal causal analysis attempts to resolve cause–effect relationships, i.e. to reveal which variables (drivers) exert a direct influence on an other variable (receiver) thereby changing its behaviour. The quantity of interpretation then is not anymore a variable value but its dependencies to other variables. While a dependence can be regarded as a binary quantity (depending—not depending), it is typically also assigned a strength, and if possible, also a direction. Thus if one assumes transpiration and photosynthesis to be coupled and regulated via a third process, i.e. stomatal conductance, as it is the case in current model implementations (De Kauwe *et al* 2013), their dependencies to atmospheric drivers would also change synchronously. A decoupling between photosynthesis and transpiration thus manifests via a divergence in their individual dependencies to atmospheric and environmental influences.

Here, to investigate the decoupling between photosynthesis and transpiration we use a causal inference method. PCMCI (a combination of the PC algorithm which is named after its inventors Peter and Clark, and the momentary conditional information, MCI; Runge *et al* 2019b) is a causal graph discovery algorithm, which has been tested and applied to eddy-covariance data in recent studies (Krich *et al*

2019, 2020). There, obtained dependence structures were interpretable even on half-hourly time resolution, and despite the inherent noisy character of eddy-covariance measurements at those scales (e.g. Hollinger and Richardson 2005, Richardson *et al* 2008). Nonetheless, a crucial drawback of the original PCMCI for its use to investigate photosynthesis–transpiration decoupling is its inability to handle contemporaneous links, i.e. variables reacting to each other in an effectively instantaneous manner (as it is the case for most biosphere–atmosphere interactions). Conveniently, the latest algorithm version, PCMCI+ (Runge 2020), is also able to attribute cause–effect relationships even when dealing with contemporaneous interactions. Therefore, using PCMCI+, we aim to revisit the hypothesis of ecosystem scale decoupling of photosynthesis and transpiration during heat events. This is achieved by investigating the dependence structure among atmospheric conditions and biosphere fluxes as measured with the eddy-covariance technique. The focus is on Australian woody ecosystems because the eddy-covariance sites experience the higher air temperatures compared to those listed in the FLUXNET2015 database (De Kauwe *et al* 2019).

2. Method and data

2.1. Data

The study by De Kauwe *et al* (2019) serves as motivation to this work, in which a more formal causal inference approach is taken. A comparison between both studies can be found in table B1. Eddy covariance data comes from the OzFlux database of woody ecosystems (L3 version) at 30 min time resolution (last accessed on 23 February 2021). The L3 version is post-processed and quality checked; the removal of spurious measurements leads to gaps in the records. We extract the following variables: Downwards shortwave (SW_IN, $\mathrm{W\,m^{-2}}$) and longwave (LW_IN, $\mathrm{W\,m^{-2}}$), and upwards longwave (LW_OUT, $\mathrm{W\,m^{-2}}$) radiation, air temperature (T_air, °C), net CO_2 flux (net ecosystem production (NEP), positive flux resembles carbon uptake, $\mu\mathrm{mol\,m^{-2}\,s^{-1}}$), water vapor deficit (VPD, kPa), surface sensible heat flux (H, $\mathrm{W\,m^{-2}}$), surface upward latent heat flux (LE, $\mathrm{W\,m^{-2}}$), soil moisture (SWC, % or $\mathrm{m^3\,m^{-3}}$, measured at the shallowest sensor 0–0.15 m) and precipitation (P, mm). Using LW_IN and LW_OUT we estimated surface temperatures (T_surface) in °C according to: $\sqrt[4]{\frac{LW\_OUT - (1-\epsilon)*LW\_IN}{\sigma/\epsilon}} - 273.15$ K (ε values are given in table A1).

Further we retained only woody sites that reach 37 °C or higher temperatures at some point during the record. This excludes Cape Tribulation, Warra, and Robson Creek. The final sample includes 13 woody ecosystems (see figure 3 and table 1).

2.2. PCMCI+

Instead of comparing variable values, we consider the strength of causal dependencies between variables. To do so, we reconstruct causal graphs using the PCMCI+ causal discovery algorithm (Runge 2020). PCMCI+ is a time-series extension of the PC algorithm (named after its inventors Peter and Clark; Spirtes and Glymour 1991). Compared to its predecessor, PCMCI (Runge *et al* 2019b), PCMCI+ can also account for contemporaneous causal effects. Here, we present a brief description of method rather than giving a full mathematical formulation, since the latter is detailed in Runge (2020).

The goal of causal discovery algorithms is to estimate time series graphical models (see figure 1(f)), where variables at different times define nodes (○) and the causal dependencies between them are visualised as edges (→).

PCMCI+ belongs to the widely-applied class of conditional independence (CI)-based causal discovery algorithms, here for the case of time series (Runge *et al* 2019a). These algorithms are based on the assumption that a statistical dependence between two variables X and Y stems from an underlying causal connection (Causal Markov Condition) and, conversely, that statistical independence indicates the absence of a causal connection (Faithfulness assumption). A causal connection in a causal graph can be direct or indirect, $X \to \cdots \to Y$ (and vice versa), or due to a confounded relation $X \leftarrow \cdots \leftarrow Z \to \cdots \to Y$. Like the PC algorithm for non-time series data, PCMCI+ assumes that no unobserved confounding variables are present. For the time series case an additional assumption is causal stationarity, i.e. if a link $X \to Y$ exists at time t, it also exists at all other times t'.

In Earth science causal sufficiency is difficult to obtain as not all required variables can be measured or are known. The obtained dependence structure thus is causally interpretable only with respect to the variables included in the analysis. This assumption can be relaxed, though, see the LPCMCI method (Gerhardus and Runge 2020). Causal stationarity is also not usually the case over long time periods, but this can be accounted for by limiting the analysis to homogeneous periods. In our analysis we use a linear CI test (partial correlation) which further assumes linear relationships and Gaussian distributions.

PCMCI+ is based on iteratively conducting CI tests. Testing for CI between X and Y given a set of variables Z is here done using partial correlations (ParCorr) (see Krich *et al* 2019, for detailed description and tests) whose significance is evaluated using a two sided t-test. The goal of PCMCI+ is to optimize the choice of conditioning sets in CI tests in order to increase detection power and at the same time maintain well-calibrated tests which is facilitated by the momentary conditional independence (MCI) test (Runge *et al* 2019b) idea.

Table 1. Ozflux sites used in the study (www.ozflux.org.au, last accessed on 23 February 2021). The different columns show the day of the year with the highest average maximum air temperature (at half hourly resolution) (doy $T_{\text{air max}}$), the beginning (start doy) and end (end doy) of the examination period, the world ecoregion classification, leaf area index (LAI) and mean annual precipitation (MAP) both from Beringer *et al* (2016). LAI of Wombat State Forest comes from Griebel *et al* (2015). Further details about the sites are given in table A1.

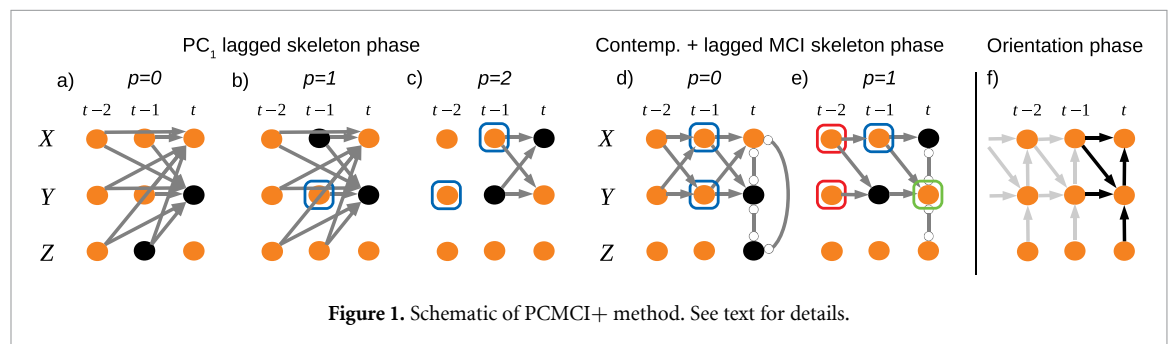| Site name	Doy $T_{\text{air max}}$	Start doy	End doy	World ecoregion	LAI $m^2\,m^{-2}$	MAP mm	$T_{\text{air max}}$ °C
Calperum	352	292	47	Mediterranean woodlands	0.5	306	48
Great Western Woodland	41	346	101	Mediterranean woodlands	0.4	361	50
Gingin	28	333	88	Mediterranean woodlands	0.9	546	46
Boyagin	20	325	80	Mediterranean woodlands	0.84	446	41
Ti Tree East	324	264	19	Deserts and xeric shrublands	0.3	259	44
Alice Springs Mulga	24	329	84	Deserts and xeric shrublands	0.3	331	43
Cow Bay	33	338	93	Tropical and sub-tropical moist broadleaf forests	4.7	3930	41
Cumberland Plain	18	323	78	Temperate woodlands	1.3	806	47
Whroo	17	322	77	Temperate woodlands	0.9	381	42
Wombat State Forest	17	322	77	Temperate broadleaf forest	1.8	924	38
Howard Springs	285	225	345	Tropical savannas	1.5	1468	39
Litchfield	282	222	342	Tropical savannas			40
Daly uncleared	285	225	345	Tropical savannas	1.2	1197	46

Figure 1. Schematic of PCMCI+ method. See text for details.

PCMCI+ consists of three phases (figure 1): (1) the PC_1 lagged skeleton phase, (2) the contemporaneous and lagged MCI skeleton phase, and (3) the orientation phase. In the PC_1 lagged skeleton phase PCMCI+ iteratively ($p = 0, 1, \ldots$) tests for CI between lagged variable pairs (black nodes) conditional on the p strongest associated variables (blue boxes, measured by their partial correlation in previous steps). After its convergence, the lagged links define the lagged conditions in the next phase. Note that at this point we may still have spurious links (here $Y_{t-1} \to X_t$ in figure 1(c). In the contemporaneous and lagged MCI skeleton phase PCMCI+ tests for CI between lagged and contemporaneous variable pairs (black nodes) conditional on the lagged conditions from the previous phase (blue boxes) as well as contemporaneous conditions (green box in figure 1(e).

In the iteration steps ($p = 0, 1, \ldots$) the cardinality of the contemporaneous conditions is increased until the algorithm converges. Finally, the information of separating sets in CI tests are used in the orientation phase resulting in a completed partially directed acyclic graph, which represents a Markov equivalence class. A Markov equivalence class contains all the causal graphs that are compatible with the conditional independencies of the data. In figure 1(f) this class has only one member, but in general some contemporaneous links may be unoriented.

As shown in Runge (2020) PCMCI+ yields much higher recall, well-controlled false positives, and faster runtime than the original PC algorithm for highly autocorrelated time series. The algorithm well exploits sparsity in high-dimensional settings and can flexibly be combined with different CI tests for

nonlinear causal discovery. PCMCI+ is available as part of the *tigramite* Python package at https://github.com/jakobrunge/tigramite.

In this work we are interested in the strength of causal dependencies. For a pair $X_{t-\tau}$ and Y_t in PCMCI+ this strength is defined as the MCI partial correlation value corresponding to the CI test with maximal p-value.

To interpret the causal strength, following Runge *et al* (2019a), consider an underlying linear causal model between Y and X where Y is determined as $Y_t = cX_{t-\tau} + \ldots + \eta_t^Y$ and $X_{t-\tau} = \ldots + \eta_{t-\tau}^X$ ('...' denotes other causal dependencies). If there is only a direct link from $X_{t-\tau}$ to Y_t, then the MCI partial correlation value is given by:

$$\rho_{X \to Y}^{\text{MCI}} = \frac{c\sigma_X}{\sqrt{\sigma_Y^2 + c^2\,\sigma_X^2}}, \qquad (1)$$

where σ_X^2 and σ_Y^2 are the variances of the noise terms $\eta_{t-\tau}^X$ and η_t^Y, respectively.
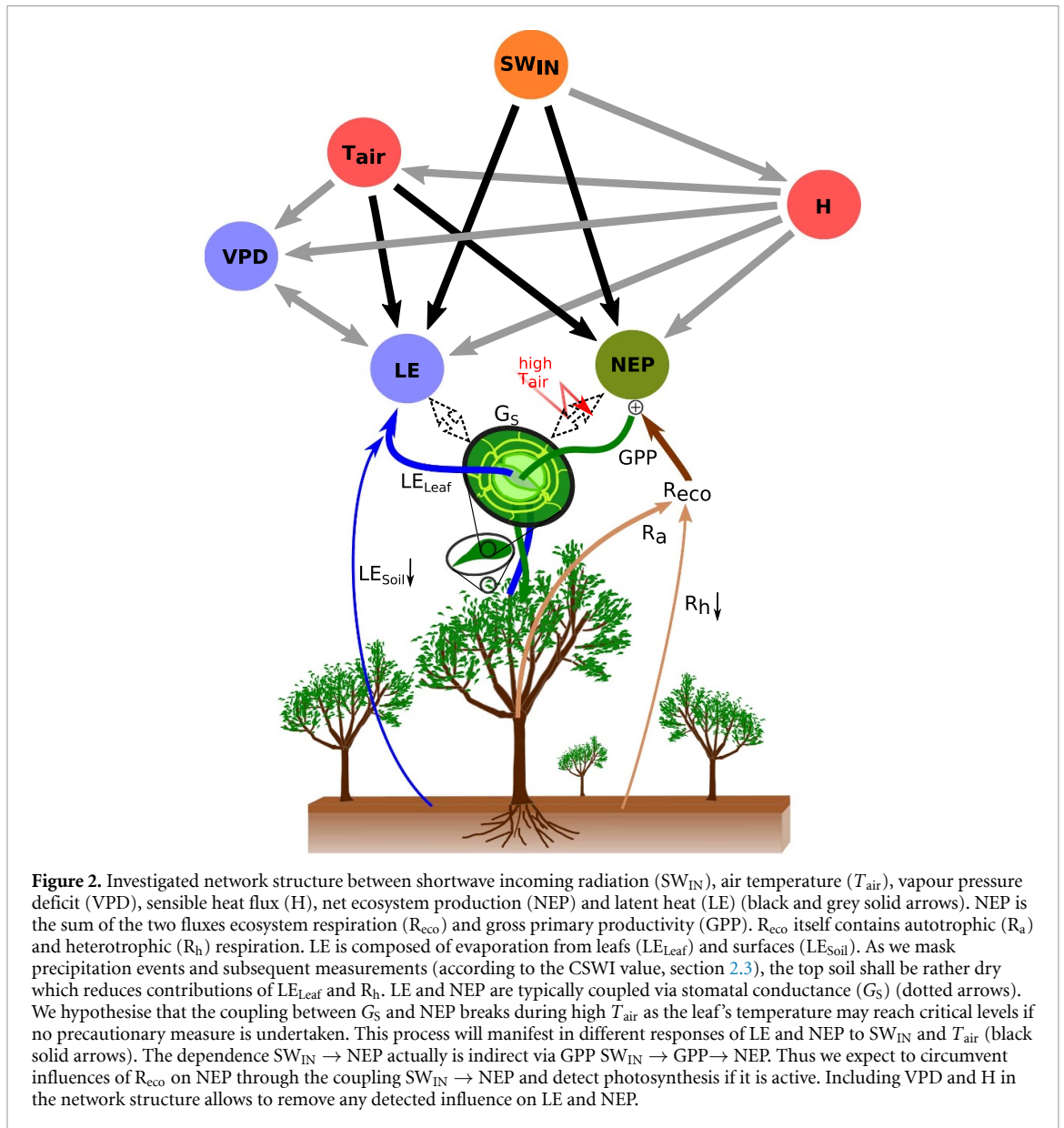
2.3. Network estimation and decoupling identification

We estimate causal graphs using PCMCI+ among the variables SW_{IN}, Ta, VPD, H, LE, and NEP at half hourly time resolution (see figure 2). NEP and LE are used as to investigate the coupling of photosynthesis and transpiration to atmospheric drivers, respectively. All measurements were flagged as missing which have a quality flag different from zero (parameter missing_flag, see table B2). Three data masks were applied to account for assumptions and approximations. Such masks lead to the removal of the data point from the analysis. First, we masked nighttime values using only data points with $SW_{IN} > 20$ W m^{-2} (figure A1(a)). Second, we only analysed 60 d before and after the day of the year with on average highest daily maximum air temperature (figure A1(b)). Third, wet surface conditions are masked out to reduce the influence of bare soil evaporation and interception loss on LE. Two approaches were used to determine wet surface conditions. First, only precipitation data is used. Here, each measurement interval with P exceeding 0.5 mm is flagged. As the surface remains potentially wet after the occurrence of precipitation the subsequent 3, 6, 9 or 12 d were masked (each option was tested to judge whether the surface is already sufficiently dry). Second, both precipitation and latent heat flux data were combined to compute the conservative surface wetness index (CSWI) (Nelson *et al* 2018)—see figure A1(a). CSWI is a simple bucket model. The bucket (depth set to 3 mm), from which water is removed half-hourly according to LE. In case of a precipitation event ($P > 0$ mm), the level is set to either the value of the previous half hour or the amount of P, depending on which is larger. Different thresholds were tested to mask out wet surface conditions (see table B2). We did not find large differences in the results using

the two approaches with the various parameter settings. Thus we present the results achieved with CSWI and a threshold of -2 mm (if not stated otherwise).

While the contribution of sources other than transpiration to LE can be largely reduced by masking out wet conditions, there is no equivalent approach to reduce the contribution of ecosystem respiration (R_{eco}) to NEP. Methods to estimate GPP from NEP measurements exist, yet they use air temperature for the estimation, which might artificially inflate the dependency of GPP on air temperature. Moreover, we are especially interested in GPP at high temperatures, and it is questionable whether the assumptions these methods are based on hold at those temperature ranges. Interestingly, in contrast to LE, the components of NEP (i.e. GPP, R_{eco}) have markedly different physical drivers: R_{eco} is largely driven by T_{air} and SWC and GPP by SW_{IN}. As long as GPP is active, it will make its fingerprint on NEP (see section 2.2) which if strong enough causes a dependence of NEP on SW_{IN} indicating active photosynthesis.

To identify a decoupling between photosynthesis and transpiration we search for deviations in the contemporaneous coupling of NEP and LE to atmospheric drivers (SW_{IN} and T_{air}), i.e. constant or even increasing link strength of LE and no or negative link strength of NEP. The decrease in NEP then is not regulated by stomatal conductance any longer but by the impairment of photosynthetic processes, which lead to an increase of CO_2 concentrations in the leaf and thus a reduction of CO_2 diffusion into the leaf due to decreasing pressure gradients. We inspect the behaviour at various temperature ranges, with particular focus on extreme high temperatures. To guarantee a sufficient amount of data points per temperature bin, while capturing especially the high temperatures as detailed as possible, we handle ecosystems individually using following procedure. We categorise the remaining non flagged data points by their T_{air} value. To find the categories, we start at the highest T_{air} value. The category's lower limit is found by decreasing the value by a certain temperature interval (ΔT_{air} and subsequently 0.1 °C) until at least a minimum of usable (non flagged) measurements (min_samples) are included in the category. A category's lower temperature limit is the high temperature limit of the next category. We decrease the temperature until 22 °C. We use various settings for min_samples and ΔT_{air} (see table B1) leading to overlapping categories with varying amounts of data points (see also Figure I1). This is intended to make the analysis more robust against random data errors. To emphasise the resulting tendency, we further aggregate the link strengths (dots in figure 4) to obtain a smother course. This aggregated metric (2 °C bins) is shown as thick lines in figure 4. Additionally, the envelope between the minimal and maximal link strength per 2 °C bin is shown as shaded areas.

Figure 2. Investigated network structure between shortwave incoming radiation (SW$_{IN}$), air temperature (T_{air}), vapour pressure deficit (VPD), sensible heat flux (H), net ecosystem production (NEP) and latent heat (LE) (black and grey solid arrows). NEP is the sum of the two fluxes ecosystem respiration (R$_{eco}$) and gross primary productivity (GPP). R$_{eco}$ itself contains autotrophic (R$_a$) and heterotrophic (R$_h$) respiration. LE is composed of evaporation from leafs (LE$_{Leaf}$) and surfaces (LE$_{Soil}$). As we mask precipitation events and subsequent measurements (according to the CSWI value, section 2.3), the top soil shall be rather dry which reduces contributions of LE$_{Leaf}$ and R$_h$. LE and NEP are typically coupled via stomatal conductance (G_S) (dotted arrows). We hypothesise that the coupling between G_S and NEP breaks during high T_{air} as the leaf's temperature may reach critical levels if no precautionary measure is undertaken. This process will manifest in different responses of LE and NEP to SW$_{IN}$ and T_{air} (black solid arrows). The dependence SW$_{IN}$ → NEP actually is indirect via GPP SW$_{IN}$ → GPP→ NEP. Thus we expect to circumvent influences of R$_{eco}$ on NEP through the coupling SW$_{IN}$ → NEP and detect photosynthesis if it is active. Including VPD and H in the network structure allows to remove any detected influence on LE and NEP.

In order to assist the causal graph estimation we do not allow links from the analysis if they are not physically plausible (parameter selected_links) as shown in figure 2. Aim was to direct as many links as possible, especially those involving NEP and LE. We do not direct the link VPD-LE as it hides a tight bidirectional connection. Further, all links pointing to SW$_{IN}$ were removed. We acknowledge the possibility of LE affecting SW$_{IN}$ via cloud formation. Yet this is expected to happen at different spatio-temporal scales than those considered here, being affected by lateral transport. The direct link SW$_{IN}$ → T_{air} is also removed, since effect of incoming solar radiation on Ta is mediated by H. Finally, due to its small diurnal variability in the absence of precipitation, SWC is not directly included in the network, but it is used to categorise the wetness conditions *a posteriori*, while interpreting the resulting network structures.

3. Results

3.1. Coupling strength in Australian ecosystems under heat stress

To investigate the behaviour of ecosystem photosynthesis and transpiration under extreme heat, we look at the coupling strength of NEP and LE to atmospheric drivers, i.e. SW$_{IN}$ and T_{air} (see section 2.3 for approximations). If both fluxes are coupled via stomatal conductance, their dependencies, i.e. the dependence strength given by the MCI value, to SW$_{IN}$ and T_{air} will change synchronously. In contrast a divergence of dependencies indicates that photosynthesis and transpiration respond differently to atmospheric influence. This behaviour would contradict a coupling via stomatal conductance. Each ecosystem has received individual T_{air} binning guaranteeing sufficient amount of data points in each bin (see section 2.3).
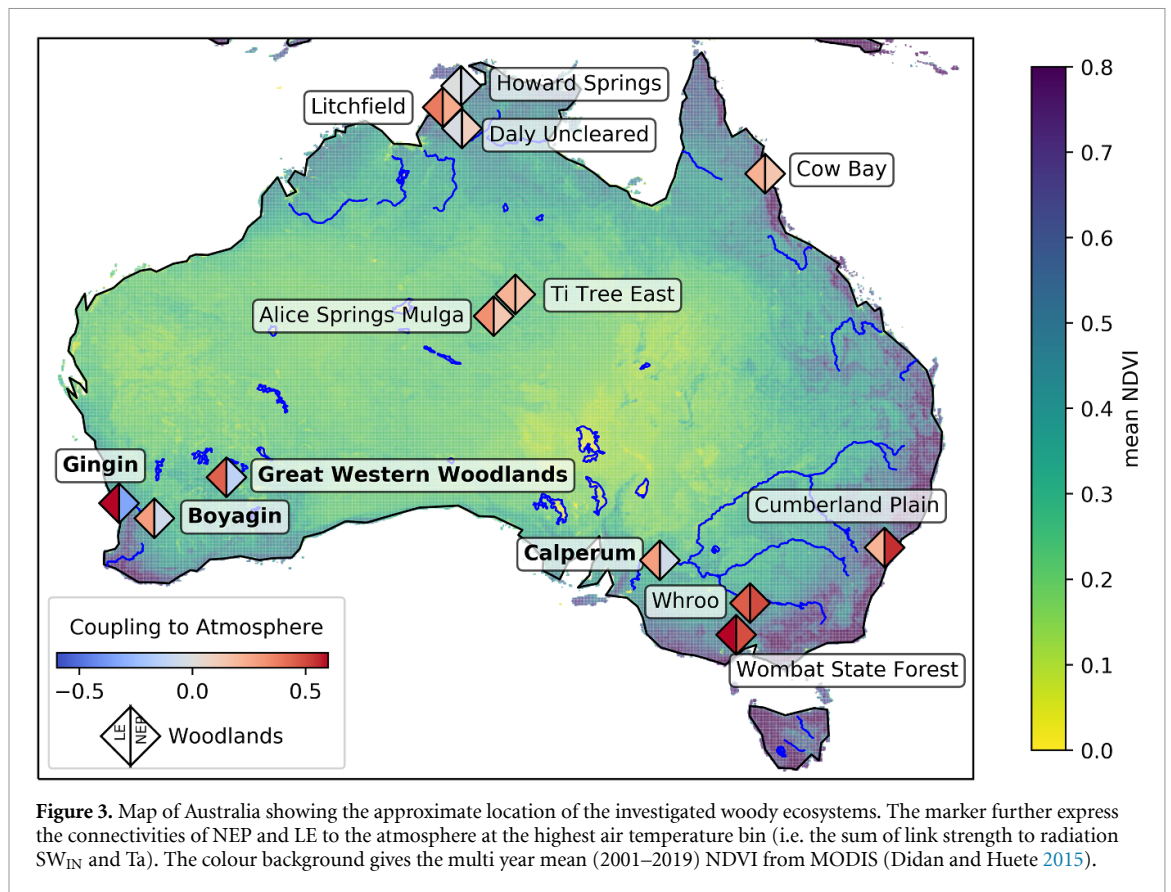
Figure 3. Map of Australia showing the approximate location of the investigated woody ecosystems. The marker further express the connectivities of NEP and LE to the atmosphere at the highest air temperature bin (i.e. the sum of link strength to radiation SW_{IN} and Ta). The colour background gives the multi year mean (2001–2019) NDVI from MODIS (Didan and Huete 2015).
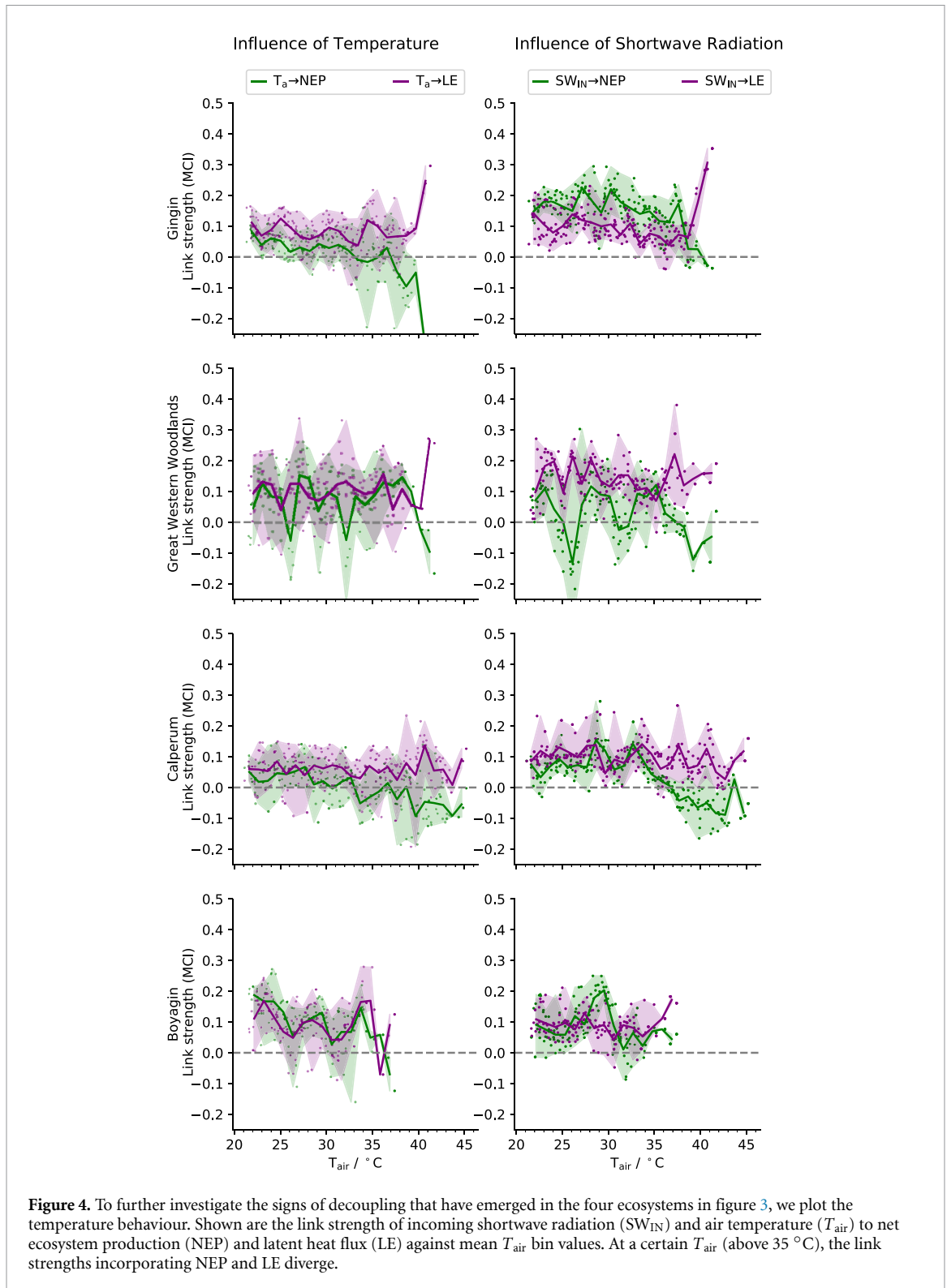
Figure 3 shows the connectivity of NEP and LE to the atmosphere at the highest temperature bin for the investigated woody ecosystems. The atmospheric connectivity of NEP and LE are simply the sum of the links $SWT_{IN} \rightarrow$ NEP, $T_{air} \rightarrow$ NEP and $SW_{IN} \rightarrow$ LE, $T_{air} \rightarrow$ LE, respectively. A decoupling shows as (rather strong) positive connectivity of LE and non or negative connectivity of NEP. This pattern is found at four ecosystems: Gingin, Great Western Woodlands, Calperum and Boyagin (ordered by the apparent strength of the decoupling). Remaining ecosystems show rather equal connectivity for NEP and LE, yet rather weak (app. 0.2) in the north and rather high (app. 0.4) in the south east. Such spatial pattern aligns with climatic conditions and vegetation types. Gingin, Great Western Woodlands, Calperum, and Boyagin can be classified as Mediterranean woodlands (MW), Cumberland Plain, Whroo and Wombat State Forest as temperate woodlands (TW), Howard Springs, Litchfield and Daly Uncleared as tropical savannas (TS), and Alice Springs Mulga and Ti Tree East as deserts and xeric shrublands (XS) Beringer *et al* (2016).

3.2. Thermal development of decoupling photosynthesis and transpiration

Next, we investigate in detail the four sites that show a more clear decoupling behaviour. Therefore we inspected the individual link strengths per T_{air} bin, starting at 22 °C (figure 4, see figures C1 and D1

for ecosystems with no effect). The maximum T_{air} reached differs across the ecosystems. Gingin, Great Western Woodlands, Calperum reach temperatures above 40 °C, Boyagin and reaches 38 °C. The link strength of $T_{air} \rightarrow$ LE and $T_{air} \rightarrow$ NEP as well as $SW_{IN} \rightarrow$ LE and $SW_{IN} \rightarrow$ NEP exhibit mostly similar values for low and medium (22 °C to app. 30 °C) temperatures. Gingin and Great Western Woodlands show a rather abrupt divergence in the way NEP and LE (green and purple lines in figure 4, respectively) interact with the atmosphere above 35 °C. Calperum exhibits a more gradual divergence starting at around 35 °C, which is characterised by a progressive decline in atmospheric connectivity of NEP (green line), while for LE the coupling to the atmosphere remains weak but rather constant at high temperature (purple line). At Boyagin, due to the rather low maximum T_{air}, the divergence is limited to a narrow temperature range between 35 °C and the maximum (around 38 °C). In contrast to the other three sites, the link $SW_{IN} \rightarrow$ NEP (green line right column figure 4) remains faintly positive (but exhibits negative values for some T_{air} bins around 32 °C).
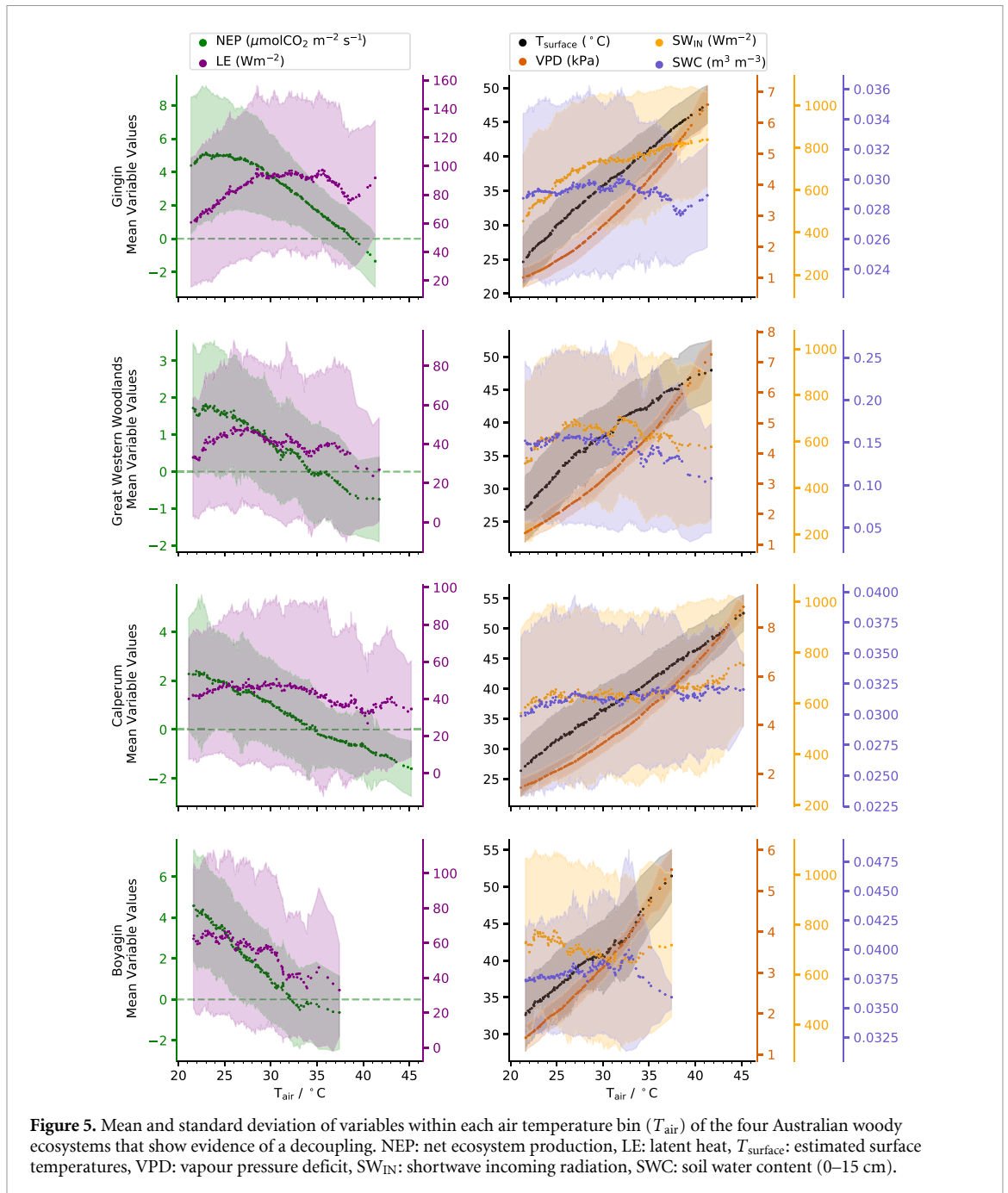
The following noteworthy patterns were observed in the variable mean values (see figure 5, see figures E1 and F1 for ecosystems with no effect): NEP of all four ecosystems turns negative (CO_2 release) approximately when $SW_{IN} \rightarrow$ NEP turns negative. At Great Western Woodlands, mean NEP decreases up to $-0.9 \, \mu mol \, m^{-2} \, s^{-1}$ and stabilises thereafter.

Figure 4. To further investigate the signs of decoupling that have emerged in the four ecosystems in figure 3, we plot the temperature behaviour. Shown are the link strength of incoming shortwave radiation (SW_{IN}) and air temperature (T_{air}) to net ecosystem production (NEP) and latent heat flux (LE) against mean T_{air} bin values. At a certain T_{air} (above 35 °C), the link strengths incorporating NEP and LE diverge.

LE changes only little with increasing T_{air} (app. 30 W m^{-2} range) in all four ecosystems. At Gingin a rather pronounced increase is observed at 38 °C (by 20 W m^{-2}). Nonetheless, LE tends to follow the patterns of mean SWC, as expected in water-limited ecosystems.

We tested various masking parameters to assess remaining effects of surface moisture on the dependencies of those ecosystems showing a decoupling. We focused on the links $T_{air} \rightarrow LE$ and $T_{air} \rightarrow NEP$

as well as $SW_{IN} \rightarrow LE$ and $SW_{IN} \rightarrow NEP$ and the mean values of NEP, LE and SWC (see figure G1). Link strengths can vary considerably across different masking parameters. The running mean (thick line) though exhibits similar patterns across CSWI values. At Great Western Woodlands, the maximum T_{air} value lies notably lower at CSWI values of -6 mm and -9 mm compared to -2 mm (since more measurements are flagged, the T_{air} bin size has to increase to incorporate min_samplesizes). Mean NEP and LE

Figure 5. Mean and standard deviation of variables within each air temperature bin (T_{air}) of the four Australian woody ecosystems that show evidence of a decoupling. NEP: net ecosystem production, LE: latent heat, $T_{surface}$: estimated surface temperatures, VPD: vapour pressure deficit, SW_{IN}: shortwave incoming radiation, SWC: soil water content (0–15 cm).

values stay rather constant, especially at Gingin. The standard deviation per T_{air} bin is slightly stronger affected showing a decrease of LE and increase of NEP in Great Western Woodlands with stricter masking. At Calperum LE actually shows a slight increase in LE with stricter masking. SWC values decrease by app. 5% and 7% in Great Western Woodlands and Calperum (despite rather constant LE). Gingin shows stable SWC values.

The chosen significance threshold pc_alpha affects the set of parents assigned to each variable. The parents of the variables X and Y enter the CI test $I(X; Y|Z)$ as the conditioning set Z. Thus we test the results sensitivity on pc_alpha (0.01, 0.05, 0.1, 0.2) using a CSWI value of -2. The results

appeared insensitive (see figure H1). We find a slight decline in link strength with increasing pc_alpha. This can be explained as the conditioning set Z tends to increase with weaker significance thresholds. A large Z decreases the detection power and thus the estimated link strength. Great Western Woodlands shows some decline in link strength of $SW_{IN} \rightarrow LE$ at high temperature but still has a positive MCI value of around 0.15.

4. Discussion and conclusion

Controlled experiments in recent years indicated the existence of a decoupling between photosynthesis and transpiration in trees at extreme high temperatures

(Schulze *et al* 1973, Ameye *et al* 2012, Urban *et al* 2017, Drake *et al* 2018). This means stomata remain conductive such that transpiration can occur or even increase, despite photosynthesis having ceased to (near) zero due to biochemical limitations. The latter typically leads to stomatal closure via an increasing internal leaf CO_2 concentration. Such mechanism can be a powerful tool to prevent heat damage in plants. Further, it can also play a crucial role to mitigate heat extremes at ecosystem level by maintaining or increasing the latent heat flux. However, conclusive evidence for the decoupling phenomenon at ecosystem scale is still incomplete (De Kauwe *et al* 2019). This is why we used a novel causal inference method to examine whether ecosystem-scale photosynthesis and transpiration can decoupling at high temperatures. Applied to eddy-covariance data, the method quantifies the coupling of carbon and water fluxes to their atmospheric drivers, and how this changes at extreme high temperatures. We could identify four sites where the latent heat flux remained coupled to atmospheric drivers while the carbon fixation decreased after a threshold of >35 °C. The formal analysis in using casual inference supported the hypothesis of a decoupling at the woody ecosystems Gingin, Great Western Woodlands, Calperum and Boyagin. The independent observation of this phenomenon at different sites makes it unlikely that this effect is an artefact e.g. due to data uncertainty. Of course, the sample size is far too small to estimate the relevance of such a process at global scale.

It is important to restate that the variables used to diagnose water and carbon fluxes, i.e. NEP and LE, are not equivalent to ecosystem photosynthesis and transpiration. Soil evaporation and respiration dynamics may hence influence the results. However, by limiting the analysis to dry surface conditions (assessed via CSWI, see section 2.3) non-transpirational sources to LE are limited. Such measures can also affect soil respiration, which decreases when soil water contents become too low and limit microbial activity (Reichstein *et al* 2006). A stricter masking of measurements after precipitation events, led to lower mean surface SWC, yet, both link strengths and values of NEP and LE remained largely unaffected (see figure G1). Thus, we consider the remaining contributions of soil respiration and surface evaporation negligible. However, autotrophic respiration also increases with temperature which can lead to a negative NEP even though photosynthesis may still be occurring, albeit at a reduced rate. The examined MW ecosystems have negative NEP at the highest T_{air}. Though, as they have also zero or negative link strength of $SW_{IN} \rightarrow$ NEP (figure 4), we assume that little to no photosynthesis occurs at highest T_{air}. This conclusion seems to contradict the findings by van Gorsel *et al* (2016) using flux-derived GPP estimates during the 'Angry

Summer', an exceptional large-scale heat wave event in southern Australia in January 2013. The authors found that GPP decreased (from app. 5 μmol m^{-2} s^{-1} to 3 μmol m^{-2} s^{-1}) during the hottest part of the heatwave but it was sufficient to yield a positive NEP at Gingin, Calperum, and Great Western Woodlands at least during morning hours. One could argue that the fingerprint of photosynthesis on NEP is critically weak during such stress events, but we show here e.g. for Cumberland Plain, which has even more negative NEP values at high T_{air} (see figure C1), a very strong link $SW_{IN} \rightarrow$ NEP which can only be explained with photosynthesis. This finding is again in line with van Gorsel *et al* (2016). Thus, for the MW ecosystems, we seem to have a discrepancy between directly flux-partitioning derived estimates of ecosystem photosynthesis and inferences considering the causal link strength.

Temporarily neglecting the discrepancy between GPP estimates and conclusions drawn from the link $SW_{IN} \rightarrow$ NEP, we question which factors could explain the decoupling of transpiration and photosynthesis at the MW ecosystems and no decoupling in remaining ecosystems? Cunningham and Read (2006) examined the leaf temperature tolerance of temperate and tropical trees from Australia at controlled laboratory conditions. A temperature range of 47 °C–54 °C was found to cause visible leaf damage in 50% of the samples after an exposure of 30 min. However, they also showed that hotter climates of origin lead to higher tolerance to extreme high temperatures. Of course temperature thresholds also depend on the exposure time (Colombo and Timmer 1992). The maximal air temperatures considered in our analysis for the MW ecosystems reach from 41 °C up to 50 °C. Leaf surface temperatures in direct radiation conditions likely exceed the air temperature. Our estimates of surface temperature ($T_{surface}$) based on longwave radiation range from 49 °C at Gingin to above 56 °C at Calperum. Air temperatures crossing 40 °C are also present in several other woody ecosystems (see figures E1 and F1). At Cumberland Plain (TW) T_{air} even reaches 47 °C, yet, the mean $T_{surface}$ only reaches 45 °C. $T_{surface}$ crosses 50 °C only in the XS ecosystems Ti Tree East and Alice Springs Mulga while T_{air} reaches (only) 44 °C and 43 °C, respectively. Based on these temperatures, we can expect that leaf temperatures in MW and XS ecosystems will reach critical limits if no precautionary measures are undertaken by the plant.

As Drake *et al* (2018) showed, even after sustained dry conditions, some trees are capable to tap into sufficient water reserves to maintain transpiration at high air temperatures and VPD, despite photosynthesis having ceased to near zero. It can be assumed that the MW ecosystems have access to some water reserves even after long deficits of rainfall. The ground water table in Gingin is at around 9 m below ground,

which may be accessible by some tree species. The very sandy soil, on the other hand, has a low water holding capacity. Meanwhile, at Calperum and Great Western Woodlands the groundwater table is expected to lie below 35 and 45 m, respectively, and in addition it is hypersaline and acidic in the case of the latter (Gray 2001). An access to groundwater reserves is thus unlikely for these two ecosystems. At Boyagin, ground water access is also unlikely. In exchange, Calperum exhibits a marked dual root system, i.e. one extensive shallow root system reaching only 50 cm depth but enabling water uptake from small rainfall events, and deep reaching roots enabling access moist silty sand between 5 m and 12 m. In addition, especially the top soil is very sandy and little aboveground biomass is present to intercept rainfall. Precipitation thus quickly infiltrates the soil Meyer *et al* (2015). At Great Western Woodlands trees exhibit an extensive network of lateral roots. Younger trees are also found to have tap roots possibly reaching down to 35 m depths (Lintern *et al* 2013). The soil has a high clay content which leads to a high water holding capacity and little effect of precipitation on soil water content at depth below 50 cm. The soil water content up to this depth is found to vary between 15% and 60% (volumetric) which corresponds roughly to 200 mm water storage. 200 mm of precipitation can occur during the largest summer storm events, which, however, cannot infiltrate the soil fully due to low permeability. Thus, considerable quantities of heavy rainfall are lost via surface runoff. To put this into perspective, given a LE of 40 W m^{-2}, the 200 mm of stored soil water content would last for roughly 140 d. While a tree height of 18 m at 360 mm mean annual precipitation may hint to some unique characteristics of Great Western Woodlands, the vegetation structure and transpiration rates of the MW ecosystems resembles those of ecosystems adapted to water scarcity.

Meyer *et al* (2015) closely investigated the evaporation at Calperum and found that this ecosystem has a very conservative water use strategy which curbed transpiration even after significant rainfall. This effect was suggested to enable the ecosystem to withstand the common dry periods of variable duration. For example, since 2017, significant precipitation capable of rewetting the upper soil layer (2.5 m) has been absent. Such restricted water use appears consistent with the largely constant but very weakly coupled latent heat flux to air temperature ($T_{air} \rightarrow$ LE) and radiation (SW$_{IN} \rightarrow$ LE)—see figure 4). Further, Meyer *et al* (2015) found the leaf area to be linked to precipitation, i.e. leaf area decreases with lasting water deficits. A decrease of leaf area with increasing temperatures has not been investigated so far in Calperum but it seems plausible, as soil water contents and air temperatures are often anti-correlated. This mechanism might give a strong hint to the underlying causes for the observed decoupling

and differences among ecosystems: If water is such a scarce resource that spending more can lead to death in the long run (as reservoirs are being depleted), increasing the effect of the amount that can be spent is the only way to survive lethal temperatures. A decrease in leaf area and stable LE leads to an increase of transpiration and thus higher cooling per leaf area.

Bearing the role of leaf area in mind, the focus shall be directed again to the question, whether the MW ecosystems can realise photosynthesis at peak temperatures. Therefore we compare the MW ecosystems with the XS ecosystems as both ecosystem types exhibit $T_{surface}$ estimates at dangerous levels. But, both link strengths including NEP as well as mean NEP values remain (slightly) positive at the XS ecosystems (Alice Springs Mulga and Ti Tree East) even at high T_{air} indicating active photosynthesis. Their mean LE at the highest T_{air} bin (43 W m^{-2}) lies slightly above those of Great Western Woodlands, Calperum and Boyagin (26, 34 and 33 W m^{-2}). With 91 W m^{-2}, mean LE appears exceptional high at Gingin at highest T_{air}, but here an increase of almost 20 W m^{-2} is observed beyond 38 °C. Based on LE values alone the XS ecosystems do not appear different. However, putting these values in relation to leaf area index (LAI) (see table 1), reveals that their transpirational cooling per unit of leaf area is considerably larger (143 W m^{-2} compared to the 101, 65, 68, 39 W m^{-2} for Gingin, Great Western Woodlands, Calperum and Boyagin, respectively). This difference can increase even further when taking the incident radiation into account. Gingin has a very high SW$_{IN}$ value of 838 W m^{-2}, approximately 200 W m^{-2} larger than the XS ecosystems and considerably higher LAI (0.9 m^2 m^{-2} compared to 0.3 m^2 m^{-2}). Assuming a homogeneous insolation of the available leaf area, Gingin would have to cope with an energy surplus per unit of leaf area that is tenfold that of XS ecosystems. These are only back-of-the-envelope calculations. However, with respect to the already high T_{air} limiting heat diffusion, they hint that the MW ecosystems are likely to be close to their thermal limits. The strong increase of LE above a T_{air} value of 38 °C at Gingin might therefore be seen as the last protective mechanism to prevent canopy dieback or maybe even plant death. Moreover, the capability to photosynthesise at such conditions is likely strongly inhibited which supports our conclusion based on the link strength SW$_{IN} \rightarrow$ NEP. More precision might be obtained using LAI values from the respective time of the year (and not annual means) as well as from using the actual leaf area exposed to direct incoming solar radiation

Notwithstanding, there are further ecosystem characteristics that deserve further scrutiny. The XS ecosystems experience a warmer climate than the MW ecosystems. Thus, conditions can favour an increased adaptation and tolerance to heat stress,

including photosynthetic processes (Colombo 1992, Colombo and Timmer 1992). The ecosystem structure can also play a crucial role in shaping characteristics of transpiration. Air temperatures can surpass 70 °C a few millimetres above ground at direct radiation conditions. Seedlings growing in such conditions must exhibit high transpiration to survive (Kolb and Robberecht 1996). Consequently, the ecosystem structure can lead to a selection of trees with high transpiration. Also, direct effects of heat on the leaf membrane could play a role. The membrane is found to become more porous, with increasing temperature increasing cuticular transpiration (Schreiber 2001, Riederer 2006). The leaf geometry itself also has significant influences on leaf temperatures and heat dissipation (Leigh *et al* 2012, 2017) which thus can help to explain observed differences among ecosystems.

In summary, using causal network estimation the coupling of transpiration and photosynthesis to atmospheric drivers is found to diverge in four out of thirteen investigated Australian woody ecosystems. The divergence is characterised by constant or even increasing responses of transpiration to radiation and air temperature despite ceasing photosynthesis. This behaviour is irreconcilable with the assumption of stomata conductance controlling both transpiration and photosynthesis simultaneously, in particular, because co-varying influences as VPD are included in the network estimation and thus accounted for. Consequently, we conclude that at the four ecosystems a decoupling occurs between photosynthesis and transpiration at ecosystem level after passing a certain temperature threshold. This means, photosynthesis has ceased due to biochemical limitations, yet stomata do not close in response to increasing internal leaf CO_2 concentrations but remain conductive allowing for transpiration to persist. Further, three

of the four decoupling ecosystems are also found by De Kauwe *et al* (2019) to show signs of decoupling. Yet, these signs were based on a bivariate comparison of daily aggregates and vanished when considering other factors. Based on surface temperature as well as leaf energy balance estimates we further hypothesise that the decoupling occurs to protect against lethal leaf temperatures. Standardised measurements are required at ecosystem or even plant level across ecosystems to further assess the proposed hypothesis as well as alternative mechanisms. Our analysis is of particular importance given that we expect future temperature extremes and extreme water scarcity to occur more often in the investigated ecosystems, which may even expand spatially in the wake of climate change.

Data availability statement

The data that support the findings of this study are openly available at the following URL/DOI: www.ozflux.org.au/.

Conflict of interest

The authors declare that they have no competing financial interests.

Appendix A. Method and data

Table A1. Further information of used Ozflux woody sites. ϵ: emissivity for $T_{surface}$ estimation. Climate class is given as Koeppen–Geiger specification.

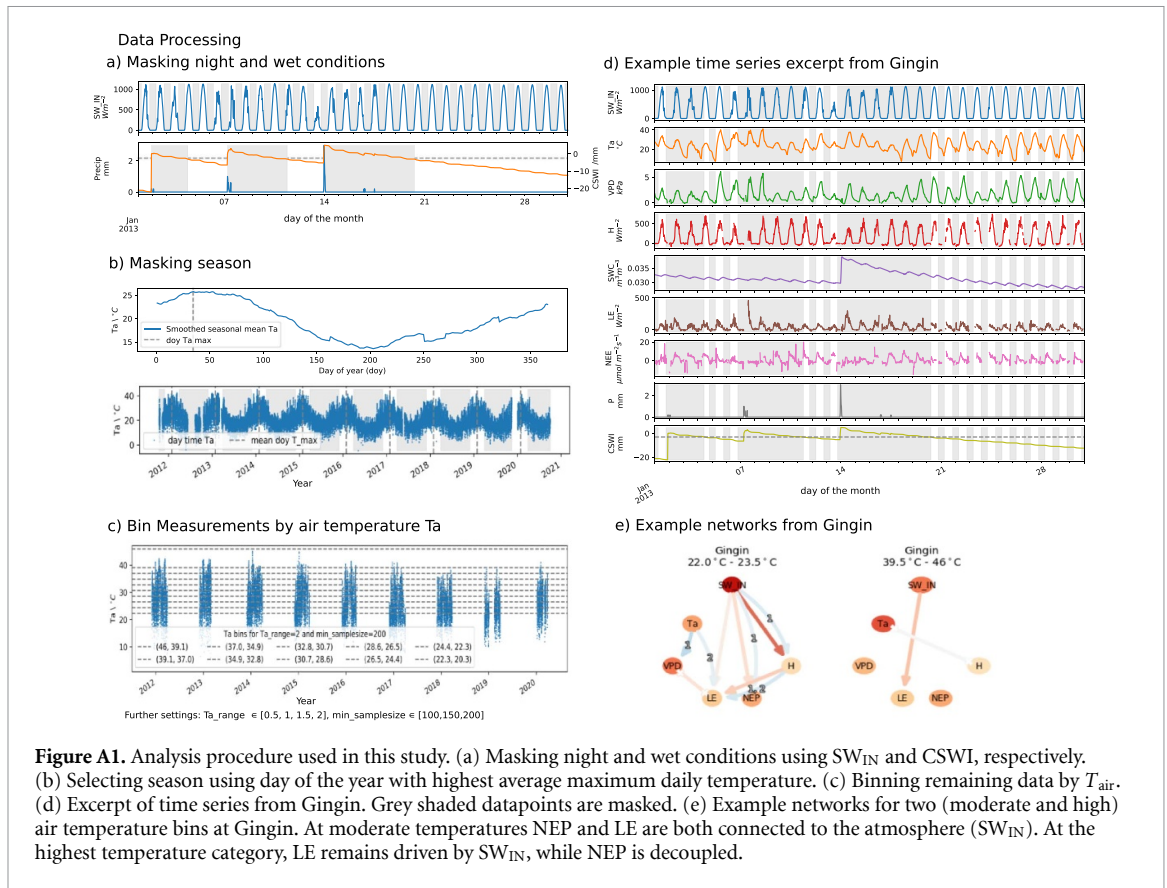| Site name	Fluxnet code	Latitude	Longitude	Date range	Vegetation type	IBRA	ϵ	Climate class
Calperum	AU-Cpr	−34.0021	140.5891	2010–2020	Semi-arid temperate eucalypt woodland	MDD	0.95	BSk
Great Western Woodland	AU-GWW	−30.1914	120.6542	2013–2020	Semi-arid temperate eucalypt woodland	COO	0.95	BWk
Gingin	AU-Gin	−31.3764	115.7138	2011–2020	Banksia woodland	SWA	0.95	Csa
Boyagin	Au-Boy	−32.4771	116.9386	2017–2020	Eucalyptus forest, broadleaf evergreen trees	JAF02	0.95	Csa
Ti Tree East	AU-TTE	−22.287	133.64	2012–2021	Hummock grass savanna with widely-spaced bloodwood trees and patches of mulga	BRT	0.95	BWh
Alice Springs Mulga	AU-ASM	−22.283	133.249	2010–2021	Mulga woodland with continuous grass understory when conditions are favourable	BRT	0.95	BWh
Cow Bay	AU-Cow	−16.2382	145.4272	2009–2019	Complex mesophyll vine forest	WET	0.97	
Cumberland Plain	AU-Cum	−33.6153	150.7236	2012–2020	Eucalyptus woodland	SYB	0.97	
Whroo	AU-Whr	−36.6732	145.0294	2011–2016	Dry sclerophyll box ironbark woodland, broadleaf evergreen trees	RIV / VIM	0.97	Cfb
Wombat State Forest	AU-Wom	−37.4222	144.0944	2010–2020	Eucalyptus forest, broadleaf evergreen trees	VIM	0.97	Cfb
Howard Springs	AU-How	−12.4952	131.1501	2001–2020	Tropical savanna (wet)	DAC	0.95	
Litchfield	AU-Lit	−13.179	130.7945	2015–2020	Tropical savanna	DAC	0.95	
Daly Uncleared	AU-DaS	−14.1592	131.3881	2007–2020	Woodland savanna	DAB	0.95	

Figure A1. Analysis procedure used in this study. (a) Masking night and wet conditions using SW_{IN} and CSWI, respectively. (b) Selecting season using day of the year with highest average maximum daily temperature. (c) Binning remaining data by T_{air}. (d) Excerpt of time series from Gingin. Grey shaded datapoints are masked. (e) Example networks for two (moderate and high) air temperature bins at Gingin. At moderate temperatures NEP and LE are both connected to the atmosphere (SW_{IN}). At the highest temperature category, LE remains driven by SW_{IN}, while NEP is decoupled.

Appendix B. Results

Table B1. Comparison of the approach of De Kauwe *et al* (2019) and our approach presented in this paper.

De Kauwe *et al* (2019)		The presented study
OxFlux, FLUXNET	Database	OxFlux
Woody ecosystems	Ecosystem types	Woody ecosystems
Daily	Data resolution	Half hourly
Masking precipitation events >0.5 mm d$^-$ and subsequent 2 d	Reducing effect of evaporation	(1) masking precipitation events >0 mm d$^-$ and subsequent 2, 4 or 6 d, (2) water balance model (CSWI), only those half hours with a CSWI below -2 mm (additionally compared to 3, 0, -1, -2, -3, -6, -9 mm)
(1) 4 d leading up to and including a day which daily maximum temperature exceeded 37 °C, (2) at least 3 consecutive days which maximum daily temperature exceeded 35 °C.	Events	Day time measurements (Rg > 20 W m^{-2}) binned by temperature starting at maximum temperature and decreased by $\Delta T_{air} \in \{0.5, 1, 1.5, 2\}$ making sure that at least min_samplesize $\in \{100\,150\,200\}$ measurements are in the bin
GPP	Carbon flux variable	NEP
LE, GPP $\times$ D$^{0.5}$	Water flux variable	LE
No	Use of SWC	Inspection of SWC behaviour with temperature; post calculation insanity check
The change in GPP and LE during (1) and GPP and GPP $\times$ D$^{0.5}$ during (2)	Method/signal of interest	Change in link strength of SW_{IN} and T_{air} to NEP and LE with increasing T_{air}; do water and carbon flux behave similar or deviate
With (1): Gingin, Great Western Woodlands, Calperum; with (2) maybe Great Western Woodlands	Ecosystems with effect	Gingin, Calperum, Great Western Woodlands, Boyagin

Table B2. PCMCI parameters that were used differently from default settings.

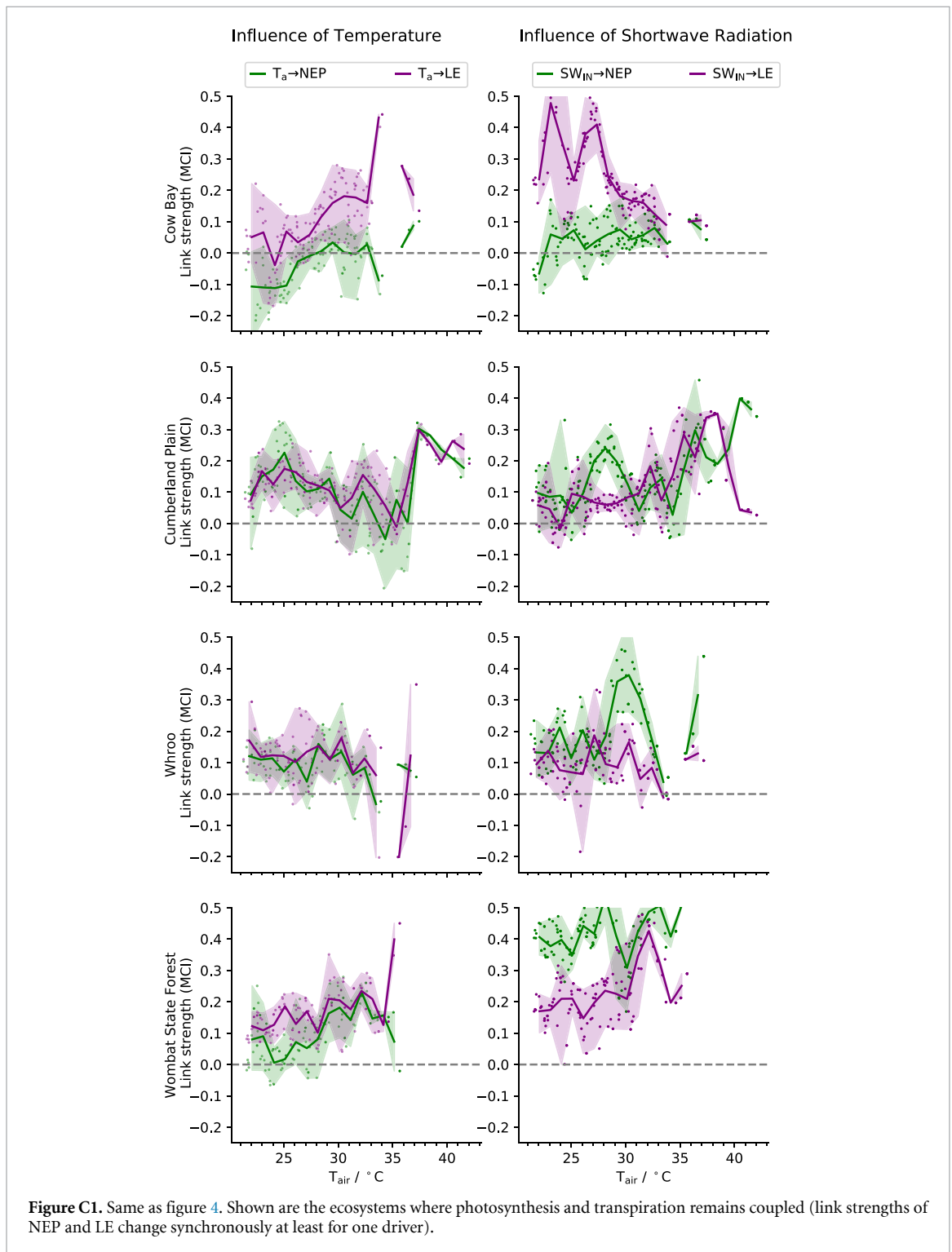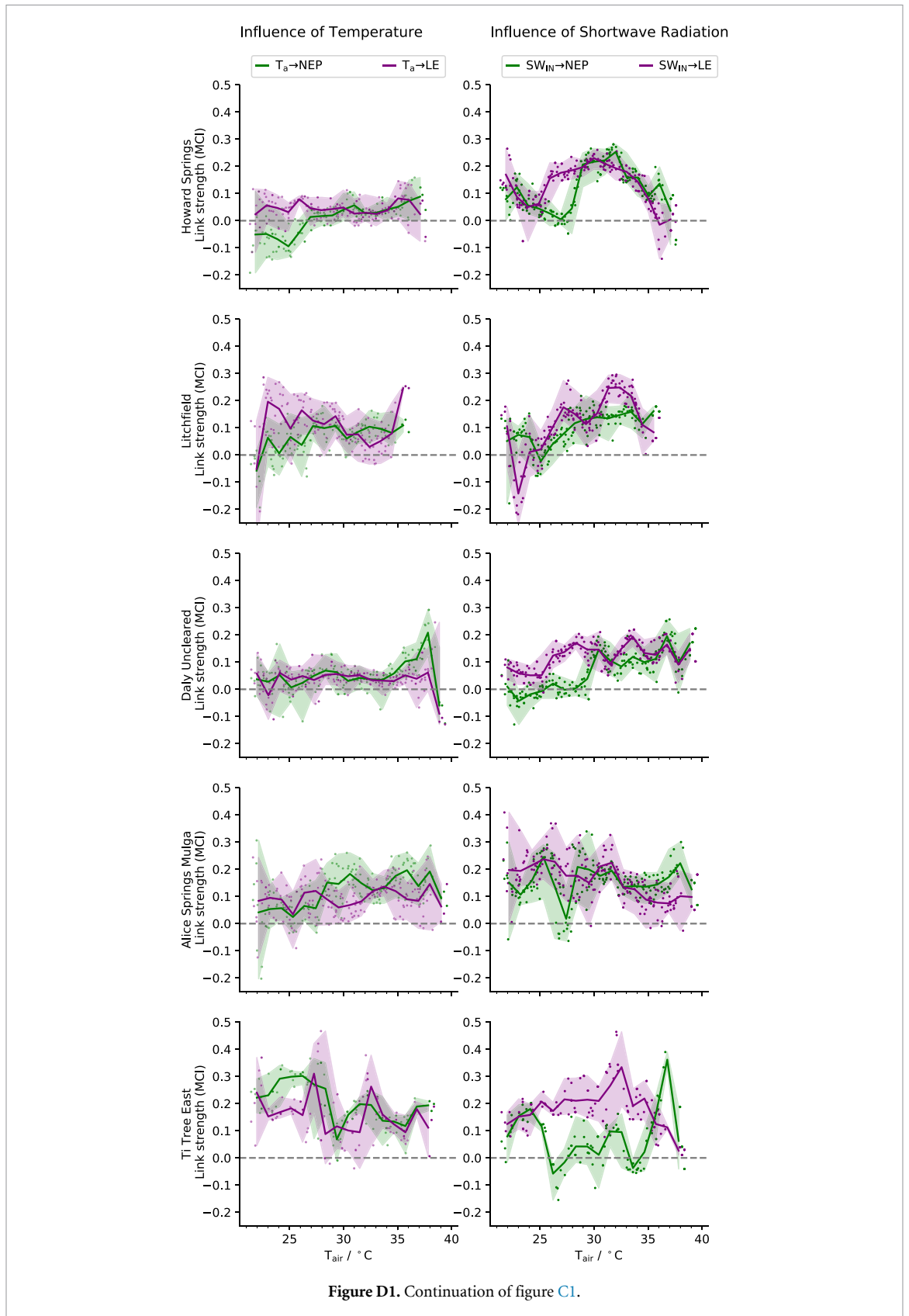| PCMCI parameter	Setting
tau_min	0
tau_max	2
pc_alpha	0.05, further tested {0.01, 0.1, 0.2}
selected_links	See figure A1, each indicated arrow is considered with lags tau_min to tau_max
mask_type	'y'
fdr_method	'fdr_bh'

Figure C1. Same as figure 4. Shown are the ecosystems where photosynthesis and transpiration remains coupled (link strengths of NEP and LE change synchronously at least for one driver).
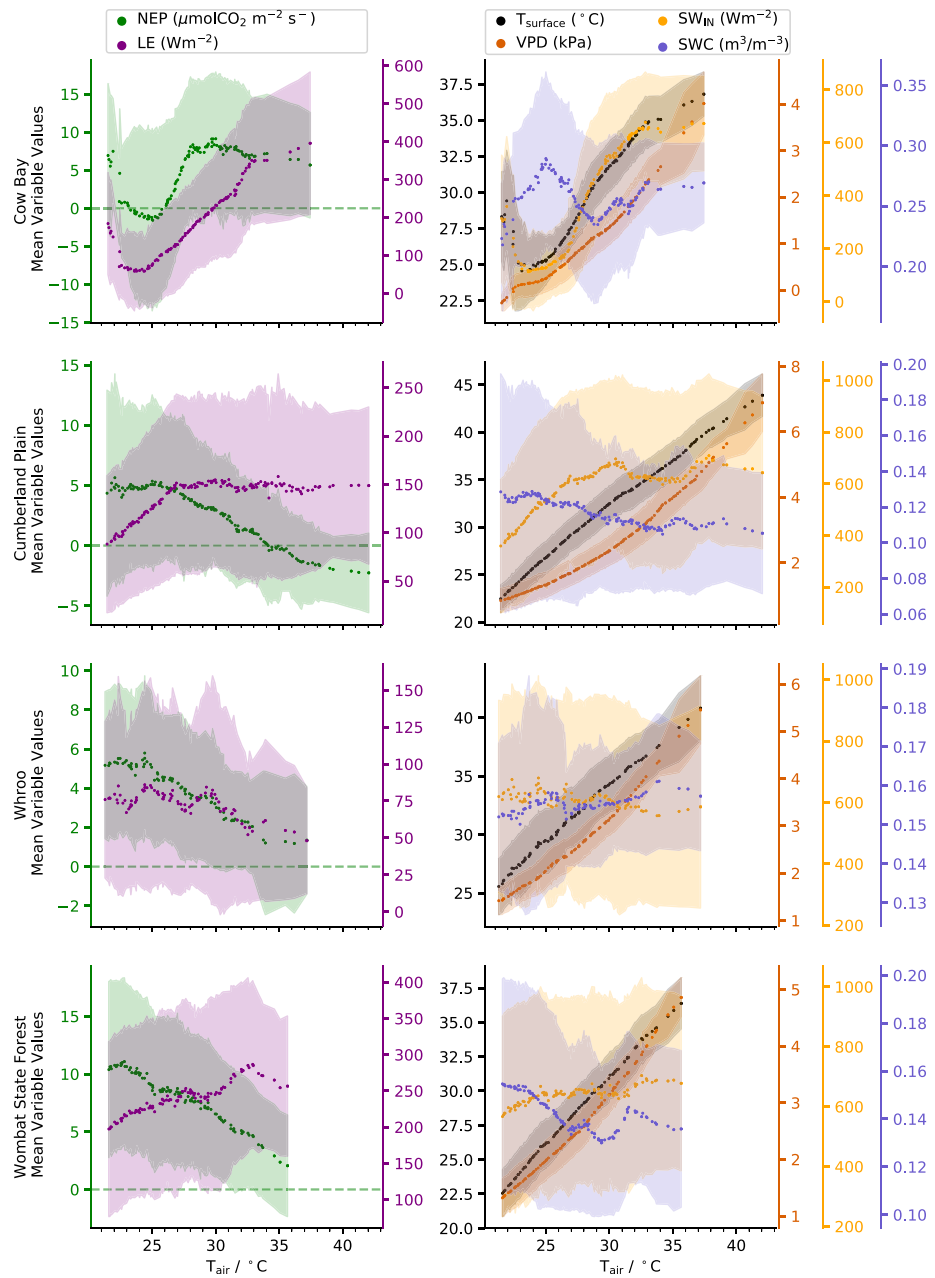
Figure D1. Continuation of figure C1.

Figure E1. Same as figure 5. Shown are the ecosystems where photosynthesis and transpiration remains coupled (link strengths of NEP and LE change synchronously at least for one driver). NEP: net ecosystem production, LE: latent heat, $T_{surface}$: estimated surface temperatures, VPD: vapour pressure deficit, SW_{IN}: shortwave incoming radiation, SWC: soil water content (0–15 cm).
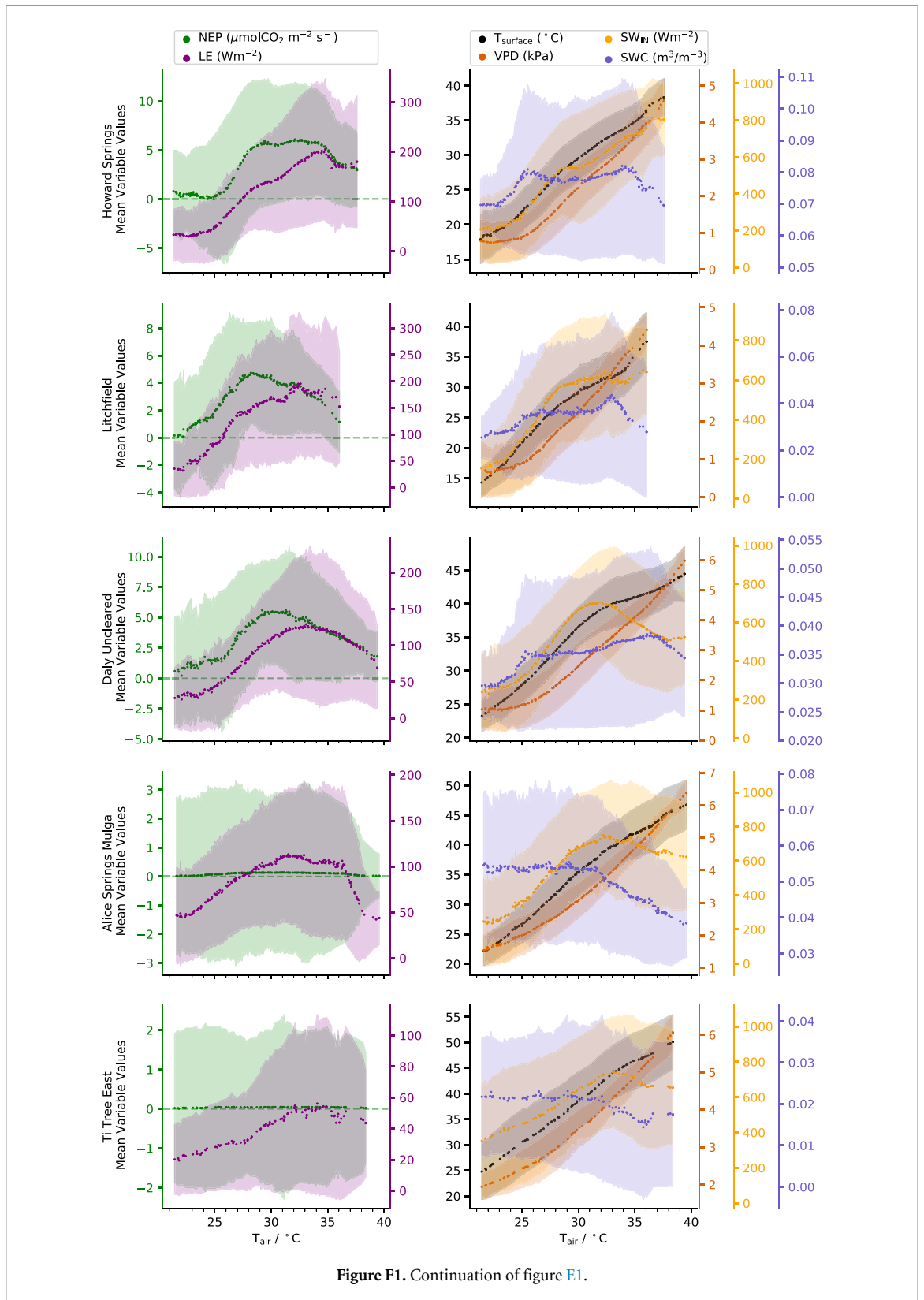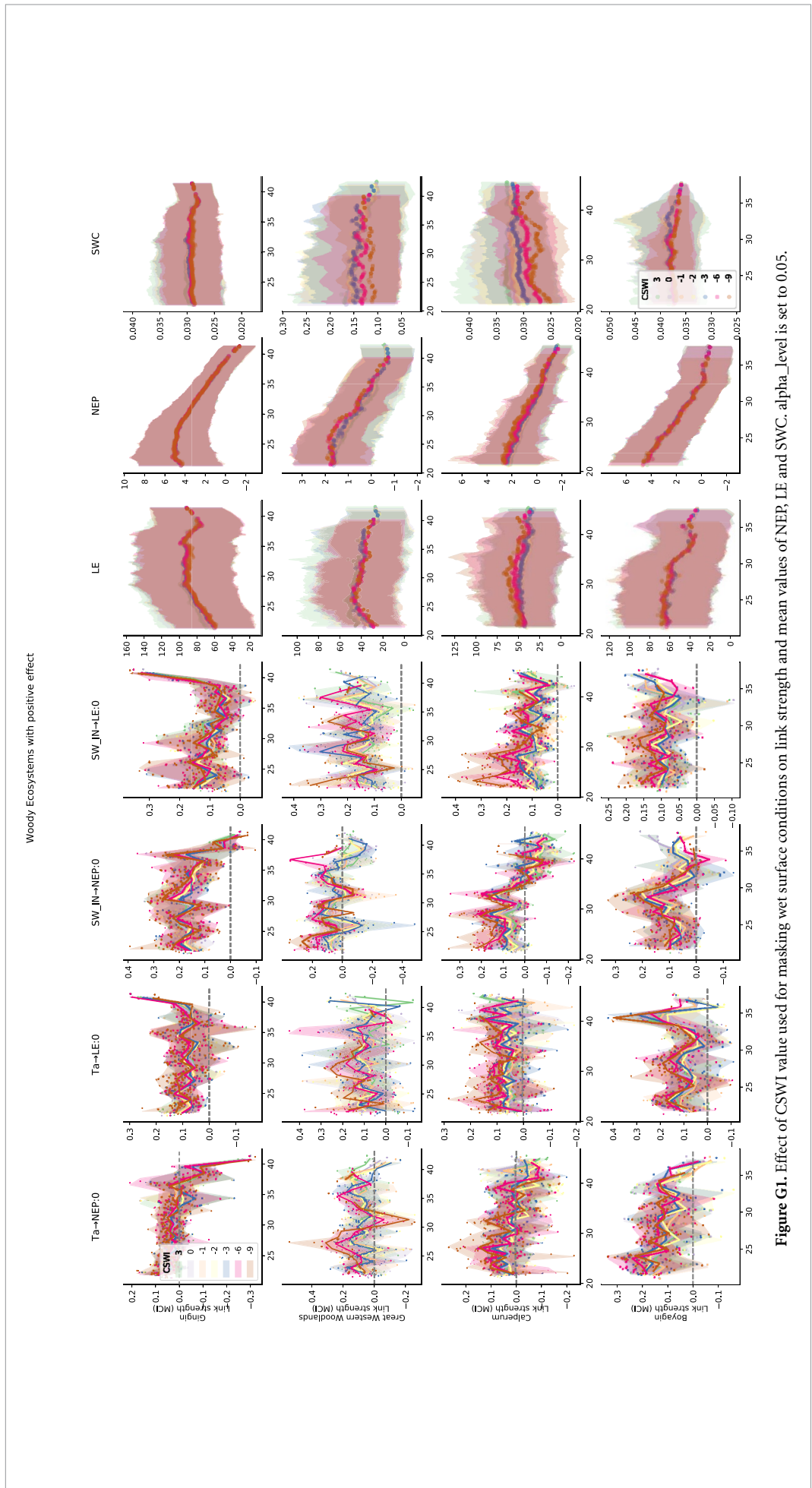
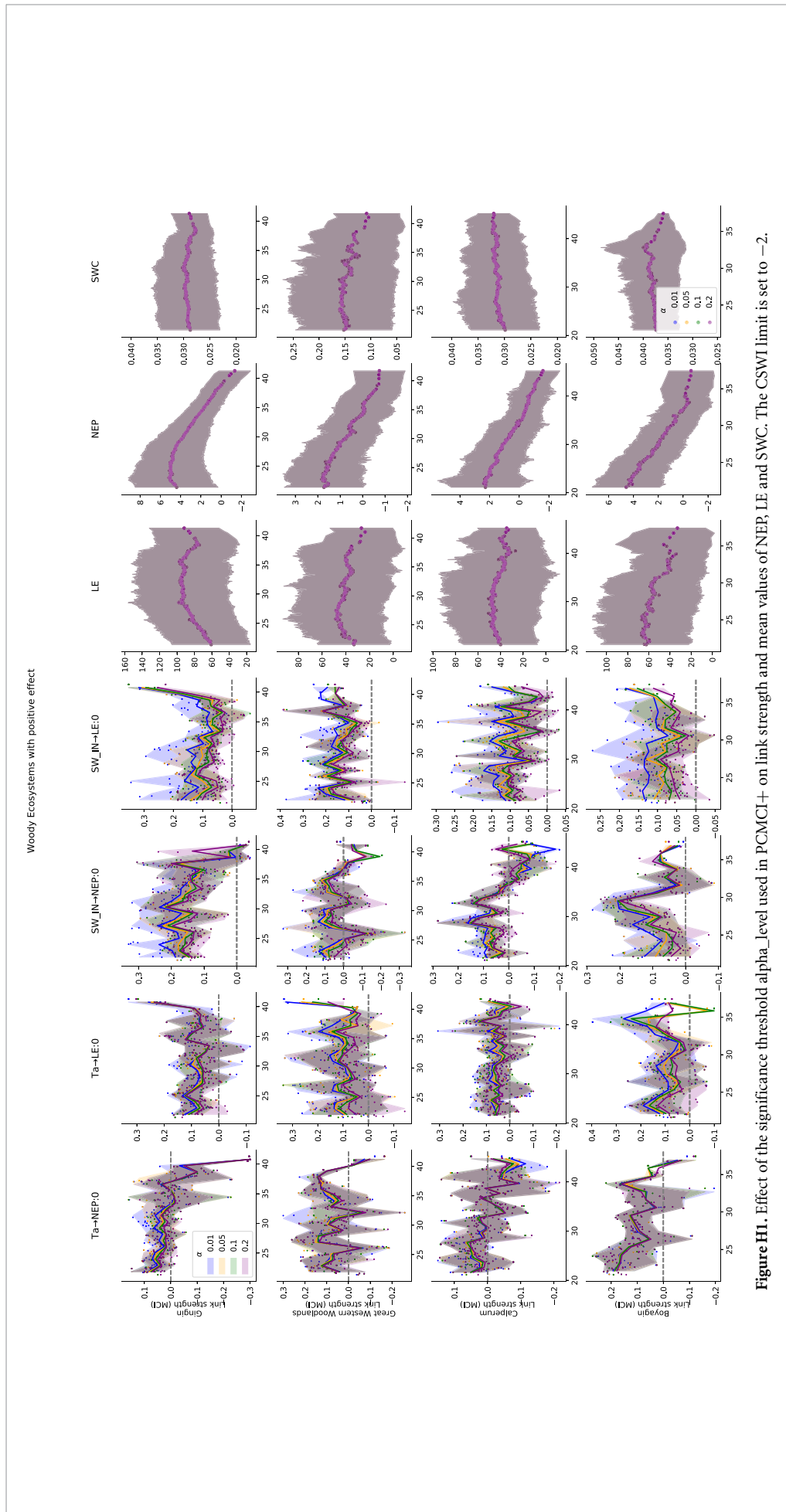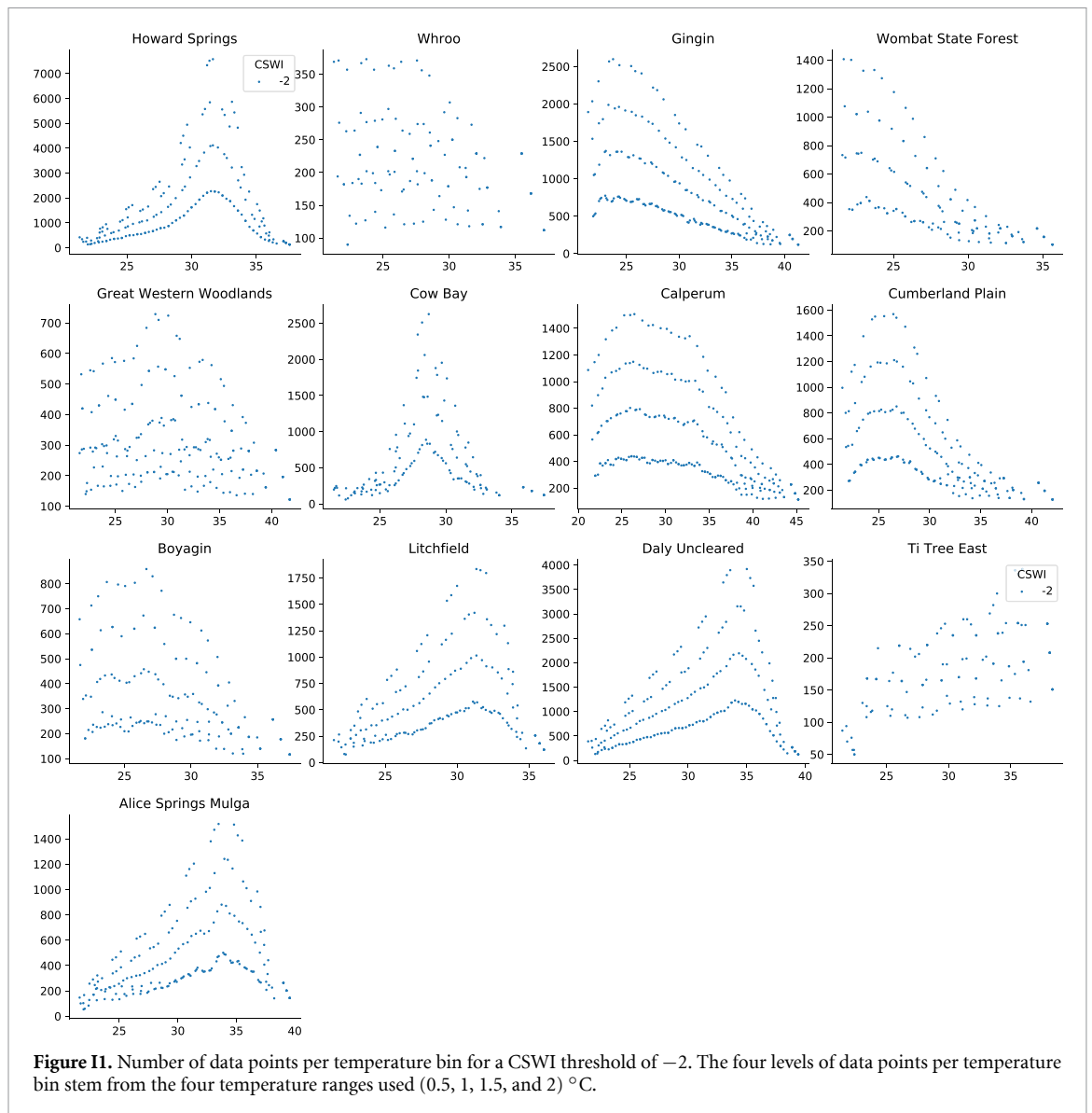**Figure F1.** Continuation of figure E1.

Figure G1. Effect of CSWI value used for masking wet surface conditions on link strength and mean values of NEP, LE and SWC. alpha_level is set to 0.05.

Figure H1. Effect of the significance threshold alpha_level used in PCMCI+ on link strength and mean values of NEP, LE and SWC. The CSWI limit is set to −2.

Figure I1. Number of data points per temperature bin for a CSWI threshold of −2. The four levels of data points per temperature bin stem from the four temperature ranges used (0.5, 1, 1.5, and 2) °C.

ORCID iDs

Christopher Krich ⬤ https://orcid.org/0000-0002-9234-0306
Miguel D Mahecha ⬤ https://orcid.org/0000-0003-3031-613X
Martin G De Kauwe ⬤ https://orcid.org/0000-0002-3399-9098
Jakob Runge ⬤ https://orcid.org/0000-0002-0629-1772
Diego G Miralles ⬤ https://orcid.org/0000-0001-6186-5751

References

Ameye M, Wertin T M, Bauweraerts I, McGuire M A, Teskey R O and Steppe K 2012 The effect of induced heat waves on *Pinus taeda* and *Quercus rubra* seedlings in ambient and elevated CO_2 atmospheres *New Phytol.* **196** 448–61

Ball J T, Woodrow I E and Berry J A 1987 A model predicting stomatal conductance and its contribution to the control of photosynthesis under different environmental conditions *Progress in Photosynthesis Research* vol 4 (Dordrecht: Springer) pp 221–4

Beringer J *et al* 2016 An introduction to the Australian and New Zealand flux tower network—OzFlux *Biogeosciences* **13** 5895–916

Colombo S J 1992 Clonal variation in heat tolerance and heat shock protein expression in black spruce MIC-93-06354/XAB Ontario Forest Research Inst., Sault Ste. Marie, ON (Canada)

Colombo S J and Timmer V R 1992 Limits of tolerance to high temperatures causing direct and indirect damage to black spruce *Tree Physiol.* **11** 95–104

Cunningham S C and Read J 2006 Foliar temperature tolerance of temperate and tropical evergreen rain forest trees of Australia *Tree Physiol.* **26** 1435–43

De Kauwe M G *et al* 2013 Forest water use and water use efficiency at elevated CO_2: a model-data intercomparison at two contrasting temperate forest FACE sites *Glob. Change Biol.* **19** 1759–79

De Kauwe M G, Medlyn B E, Pitman A J, Drake J E, Ukkola A, Griebel A, Pendall E, Prober S and Roderick M 2019 Examining the evidence for decoupling between photosynthesis and transpiration during heat extremes *Biogeosciences* **16** 903–16

Didan K and Huete A 2015 *MOD13C2/Terra Vegetation Indices Monthly L3 Global 0.05Deg CMG* (NASA LP DAAC) (available at: http://doi.org/10.5067/MODIS/MOD13C2.006)

Drake J E *et al* 2018 Trees tolerate an extreme heatwave via sustained transpirational cooling and increased leaf thermal tolerance *Glob. Change Biol.* **24** 2390–402

Gerhardus A and Runge J 2020 High-recall causal discovery for autocorrelated time series with latent confounders (arXiv:2007.01884)

Gray D 2001 Hydrogeochemistry in the Yilgarn Craton *Geochem. Explor. Environ. Anal.* **1** 253–64

Griebel A, Bennett L T, Culvenor D S, Newnham G J and Arndt S K 2015 Reliability and limitations of a novel terrestrial laser scanner for daily monitoring of forest canopy dynamics *Remote Sens. Environ.* **166** 205–13

Griebel A, Bennett L T, Metzen D, Pendall E, Lane P N and Arndt S K 2020a Trading water for carbon: Maintaining photosynthesis at the cost of increased water loss during high temperatures in a temperate forest *J. Geophys. Res. Biogeosci.* **125** e2019JG005239

Griebel A, Metzen D, Boer M M, Barton C V, Renchon A A, Andrews H M and Pendall E 2020b Using a paired tower approach and remote sensing to assess carbon sequestration and energy distribution in a heterogeneous sclerophyll forest *Sci. Total Environ.* **699** 133918

Hollinger D Y and Richardson A D 2005 Uncertainty in eddy covariance measurements and its application to physiological models *Tree Physiol.* **25** 873–85

Kolb P F and Robberecht R 1996 High temperature and drought stress effects on survival of *Pinus ponderosa* seedlings *Tree Physiol.* **16** 665–72

Krich C, Runge J, Miralles D G, Migliavacca M, Perez-Priego O, El-Madany T, Carrara A and Mahecha M D 2019 Causal networks of biosphere–atmosphere interactions *Biogeosci. Discuss.* **2019** 1–43

Krich C, Runge J, Miralles D G, Migliavacca M, Perez-Priego O, El-Madany T, Carrara A and Mahecha M D 2020 Estimating causal networks in biosphere–atmosphere interaction with the PCMCI approach *Biogeosciences* **17** 1033–61

Leigh A, Sevanto S, Ball M C, Close J D, Ellsworth D S, Knight C A, Nicotra A B and Vogel S 2012 Do thick leaves avoid thermal damage in critically low wind speeds? *New Phytol.* **194** 477–87

Leigh A, Sevanto S, Close J D and Nicotra A 2017 The influence of leaf size and shape on leaf thermal dynamics: does theory hold up under natural conditions? *Plant Cell Environ.* **40** 237–48

Leuning R 1995 A critical appraisal of a combined stomatal-photosynthesis model for C3 plants *Plant Cell Environ.* **18** 339–55

Lintern M, Anand R, Ryan C and Paterson D 2013 Natural gold particles in Eucalyptus leaves and their relevance to exploration for buried gold deposits *Nat. Commun.* **4** 1–8

Meyer W S, Kondrlovà E and Koerber G R 2015 Evaporation of perennial semi-arid woodland in southeastern Australia is adapted for irregular but common dry periods *Hydrol. Process.* **29** 3714–26

Nelson J A *et al* 2020 Ecosystem transpiration and evaporation: insights from three water flux partitioning methods across FLUXNET sites *Glob. Change Biol.* **26** 6916–30

Nelson J, Carvalhais N, Cuntz M, Delpierre N, Knauer J, Ogée J, Migliavacca M, Reichstein M and Jung M 2018 Coupling water and carbon fluxes to constrain estimates of transpiration: the TEA algorithm *J. Geophys. Res. Biogeosci.* **123** 3617–32

O'sullivan O S *et al* 2017 Thermal limits of leaf metabolism across biomes *Glob. Change Biol.* **23** 209–23

Peters J, López R, Nolf M, Hutley L, Wardlaw T, Cernusak L and Choat B 2021 Living on the edge: a continental-scale assessment of forest vulnerability to drought *Glob. Change Biol.* **27** 3620–41

Reichstein M *et al* 2006 Reduction of ecosystem productivity and respiration during the European summer 2003 climate anomaly: a joint flux tower, remote sensing and modelling analysis *Glob. Change Biol.* **13** 634–51

Reichstein M, Stoy P C, Desai A R, Lasslop G and Richardson A D 2012 Partitioning of net fluxes *Eddy Covariance: A Practical Guide to Measurement and Data Analysis* (Dordrecht: Springer) pp 263–89

Richardson A D *et al* 2008 Statistical properties of random CO_2 flux measurement uncertainty inferred from model residuals *Agric. For. Meteorol.* **148** 38–50

Riederer M 2006 Thermodynamics of the water permeability of plant cuticles: characterization of the polar pathway *J. Exp. Bot.* **57** 2937–42

Runge J *et al* 2019a Inferring causation from time series in Earth system sciences *Nat. Commun.* **10** 2553

Runge J 2020 Discovering contemporaneous and lagged causal relations in autocorrelated nonlinear time series datasets *Conf. on Uncertainty in Artificial Intelligence* (PMLR) pp 1388–97

Runge J, Nowack P, Kretschmer M, Flaxman S and Sejdinovic D 2019b Detecting and quantifying causal associations in large nonlinear time series datasets *Sci. Adv.* **5** eaau4996

Schreiber L 2001 Effect of temperature on cuticular transpiration of isolated cuticular membranes and leaf discs *J. Exp. Bot.* **52** 1893–1900

Schulze E-D, Lange O, Kappen L, Buschbom U and Evenari M 1973 Stomatal responses to changes in temperature at increasing water stress *Planta* **110** 29–42

Spirtes P and Glymour C 1991 An algorithm for fast recovery of sparse causal graphs *Soc. Sci. Comput. Rev.* **9** 62–72

Urban J, Ingwers M, McGuire M A and Teskey R 2017 Increase in leaf temperature opens stomata and decouples net photosynthesis from stomatal conductance in *Pinus taeda* and *Populus deltoides x nigra J. Exp. Bot.* **68** 1757–67

van Gorsel E *et al* 2016 Carbon uptake and water use in woodlands and forests in southern Australia during an extreme heat wave event in the "Angry Summer" of 2012/2013 *Biogeosciences* **13** 5947–64

von Caemmerer S and Evans J R 2015 Temperature responses of mesophyll conductance differ greatly between species *Plant Cell Environ.* **38** 629–37